Model for the onset of transport in systems with distributed thresholds for conduction

Klara Elteto, Eduard G. Antonyan, T. T. Nguyen, and Heinrich M. Jaeger

James Franck Institute and Department of Physics, University of Chicago, Chicago, Illinois 60637, USA

(Received 20 July 2004; revised manuscript received 9 September 2004; published 28 February 2005)

We present a model supported by simulation to explain the effect of temperature on the conduction threshold in disordered systems. Arrays with randomly distributed local thresholds for conduction occur in systems ranging from superconductors to metal nanocrystal arrays. Thermal fluctuations provide the energy to overcome some of the local thresholds, effectively erasing them as far as the global conduction threshold for the array is concerned. We augment this thermal energy reasoning with percolation theory to predict the temperature at which the global threshold reaches zero. We also study the effect of capacitive nearest-neighbor interactions on the effective charging energy. Finally, we present results from Monte Carlo simulations that find the lowest-cost path across an array as a function of temperature. The main result of the paper is the linear decrease of conduction threshold with increasing temperature: $V_t(T) = V_t(0)[1 - 4.8k_B T P(0)/p_c]$, where $1/P(0)$ is an effective charging energy that depends on the particle radius and interparticle distance, and p_c is the percolation threshold of the underlying lattice. The predictions of this theory compare well to experiments in one- and two-dimensional systems.

I. INTRODUCTION

In many physical systems, local barriers prevent the onset of steady-state motion or conduction unless a certain minimum threshold for an externally applied driving force or bias is exceeded. Often, the strength of those barriers varies throughout the system and only their statistical distribution is known. A key issue then concerns how the global threshold for onset of motion is related to the distribution of local threshold values. Examples include the onset of resistance due to depinning of fluxline motion in type-II superconductors, the onset of mechanical motion in coupled frictional systems such as sand piles, and the onset of current flow through networks of tunnel junctions in the Coulomb blockade regime. In all of these cases, defects in the host material or the underlying substrate produce local traps or barriers of varying strength.

Under an applied driving force, fluxlines, mobile particles or charge carriers from an external reservoir can penetrate the disordered energy landscape, becoming stuck at the traps or piling up in front of barriers. With increased drive, particles can surmount some of the barriers and penetrate further. However, a steady-state flow is only established once there is at least one continuous path connecting one side of the system with the other. The onset of steady-state transport then corresponds to finding the lowest-energy system-spanning path. This optimization problem was addressed in 1993 in a seminal paper by Middleton and Wingren (MW).[1]

Using analytical arguments as well as computer simulations, MW found that, for the limit of negligible thermal energies, the onset of system-spanning motion corresponds to a second order phase transition as a function of applied bias. The global threshold value scales with distance across the system, but is independent of the details of the barrier size distribution. Beyond threshold, more paths open up and the overall transport current increases. As a result, the steady-state transport current displays power law scaling as a function of excess bias. These predictions have subsequently been used extensively in the interpretation of single electron

tunneling data from networks of lithographically defined junction arrays[2,3] as well as from self-assembled nanoparticle systems.[4–6] In addition, recent experiments[7] and simulations[8] have explored how the power law scaling is affected by structural disorder in the arrays. The regime of large structural disorder and significant voids in the array was investigated numerically using a percolation model.[9]

What happens at finite temperature? Intuitively, one might expect temperature to produce a smearing of the local thresholds and thus a quick demise of the power law scaling for $T > 0$. Indeed, a number of experiments have found that the nonlinear current-voltage characteristics observed at the lowest temperatures give way to nearly linear, Ohmic behavior once T is raised to a few dozen kelvin.[10,11] More recently, however, several experiments showed that the scaling behavior survives with a well-defined, albeit now temperature-dependent, global threshold. In a previous Letter, we demonstrated for a two-dimensional metal nanocrystal array that (a) the threshold is only weakly temperature dependent, decreasing linearly with increasing T and (b) the scaling exponent remains unaffected by temperature. Consequently, the shape of the nonlinear response as a function of applied drive remains constant and is merely shifted to lower drive values as T increased.[12]

Similar behavior was also observed in small 2D metal nanoparticle networks by Ancona *et al.*[5] and Cordan *et al.*[13] and in 1D chains of carbon particles by Bezryadin *et al.*[14] Most recently, it was corroborated by simulations of (semiclassical) particles in 2D arrays of pinning sites with random strengths.[15] This weak temperature dependence of the nonlinear response also has important practical consequences as it implies that arrays are much more robust and forgiving as compared to systems with a single threshold that might be significantly affected by its local environment.

However, the theoretical approach developed by MW considers only the zero-temperature limit where the local energy levels are sharply delineated and barriers between adjacent sites are well defined. In Ref. 12 we introduced the main results from a new model that extends the MW approach to

finite temperatures. Here, we develop this model in more detail, providing both analytical results and data from computer simulations. For concreteness, we focus on single electron tunneling through metal nanoparticle arrays. However, we expect the main results to carry over to a much wider class of systems with distributed thresholds due to quenched disorder.

Our model goes beyond previous work in two important aspects. First, we introduce a method that allows us to treat finite temperatures. This method is based on estimating when small barriers, washed out by temperature, have percolated across the system, and it establishes an upper limit on the global threshold as a function of temperature. A key finding is that random quenched disorder leads to universal behavior that is independent of the details of the barrier height distribution. Second, we include nearest neighbor capacitive coupling. This leads us to a new definition of the relevant effective charging energy for system crossing, in terms of the most probable value in the distribution of energy costs. As shown in Ref. 12, the model captures the experimentally observed temperature dependence of the drive-response characteristics and predicts the collapse of the global threshold as a function of temperature on a universal curve that is independent of local junction parameters.

The paper is organized as follows. In Sec. II we outline the basic ingredients of our model, mainly focusing on the limit of negligible interparticle coupling. Section III then calculates the shape of the probability distribution of energy costs for the general case of finite nearest neighbor coupling. In Sec. IV we present simulation results for various network geometries. We also discuss the validity of the percolation model and show numerical results for the decrease of the threshold with temperature. Section V describes how the current-voltage characteristics behave at temperatures above the point where the voltage threshold reaches zero. Section VI contains a discussion of the model and comparisons with recent experimental data and as well as with numerical results from related systems.

II. THE BASIC MODEL IN THE ABSENCE OF INTERPARTICLE CAPACITIVE COUPLING

We consider one- or two-dimensional arrays of spherical metal nanoparticles ("sites"), placed between two in-plane metal electrodes. We ignore any particle-internal level spacing due to quantum size effects and treat each site as possessing a continuous spectrum of available states up to some local chemical potential. This is a reasonable approximation for metal particles with diameters larger than a couple nanometers at temperatures above liquid helium. For such particles, the largest energy besides thermal energy is the electrostatic energy associated with the transfer of additional, single electrons.

We consider interparticle spacings small enough to allow for such transfer by electron tunneling. We make the usual assumptions of the "orthodox theory" of single electron tunneling (see, e.g., Likharev in Ref. 16), namely that the tunnel time is negligible in comparison with all other time scales, the tunnel resistance $R \gg R_q = h/e^2$, where R_q is the quantum

of resistance, cotunnel events due to coherent quantum processes can be ignored, and the local tunnel rate from site to site depends only on the change in electrostatic free energy of the system, ΔE, that would result from a tunnel event. At low temperatures, a positive ΔE implies a suppression of tunneling (Coulomb blockade), and current flows only after an external bias has been applied that compensates for this energy cost. If tunneling occurs from a site at higher energy to one at lower energy ($\Delta E < 0$), we assume that the energy difference is lost due to scattering processes in the destination particle (inelastic tunneling).

Throughout the paper, we consider the limit of negligible structural disorder of the arrays, i.e., all sites are identical in terms of both their tunnel coupling and capacitive coupling to neighbors, as well as in their self-capacitance. Disorder enters in form of a random distribution of the local chemical potentials at every site due to quenched offset charges. This quenched charge disorder models charge fluctuations due to impurities in the substrate which in turn polarize the nanoparticles.

A corresponding experimental system can be realized as shown in Ref. 12 by self-assembling, onto an insulating substrate, ligand-coated nanoparticles from solution. The ligands prevent nanoparticle sintering and well-ordered arrays are formed through a balance between attractive van der Waals forces and repulsive steric hindrance between ligands from neighboring particles. For dodecanethiol ligands and particle diameters in the range 4.5 nm to 7 nm, a size dispersion of less than 5% can be achieved, resulting in 2D arrays with excellent long-range order of the particle packing. Electronic measurements, both on nanoparticle arrays but also on self-assembled monolayers of molecules by themselves, have shown that alkanethiol ligands act as mechanical spacers and do not otherwise affect the transport properties.[17,18] Consequently, they set the width of the tunnel barrier between neighboring nanoparticles but do not introduce states inside the barrier.

The quenched charge disorder is not a perturbative effect: in principle, the chemical potential of a nanoscale particle can be shifted by a nearby trapped charge as much as it would be by an added mobile electron. Therefore, electrons in an array propagate through a network of junctions with randomly varying threshold voltages. Note that the mobile charges are quantized (electrons) and thus move the local chemical potential by the same amount, $\Delta \mu$, every time a single charge enters or leaves a site. On the other hand, the quenched charges model a polarization effect and thus can move the local chemical potentials continuously, just like a local gate electrode could. The overall energy cost, ΔE, associated with a tunnel event therefore has to take into account the effect of both discrete mobile charges and of a continuous random distribution of quenched charges.

One might expect conduction through large arrays to depend on the details of the local quenched, or background, charge distribution. However, zero-temperature arguments by MW indicate that this is not the case,[1] at least in the limit of negligible capacitive coupling between sites. Instead, the overall array current-voltage characteristics (IVs) appear to be robust to background charge disorder and exhibit a nonzero effective voltage threshold, V_t, that scales linearly with array size (i.e., distance between electrodes).

To see this, consider first a 1D array at $T=0$ with a given distribution of quenched polarization charge values. Because mobile electrons can compensate for local polarizations in integer multiples of e, the electronic charge, only disorder in the range $[-e/2, +e/2]$ needs to be considered. Starting from an initial state of zero applied overall bias, mobile charges can penetrate, say from the left, single file into the disordered potential landscape until they first encounter a local up-step in electrostatic potential, $\Delta V > 0$. At this point, the Coulomb blockade prevents further advance.

To the left of the up-step, each site now has one additional charge on it and all potentials have been raised uniformly by e/C_0 where C_0 is the self-capacitance of each site. In order to move the charge front further toward the right electrode, the bias applied to the left electrode has to be raised. Each time an up-step is encountered anywhere in the array, a bias increment of e/C_0 at the left electrode will suffice to advance the front. Thus the minimum bias required in order for mobile charges to make it all the way across the array will be given by the number of up-steps times e/C_0 (recall that down-steps in local potential do not matter as tunneling is assumed to be inelastic). In other words, the $T=0$, global threshold for conduction for an array of N sites is given by Ref. 1 as

$$V_t(0) = \alpha N e / C_0. \tag{1}$$

If we now assume a flat, random distribution of quenched charges, on average half of the steps between neighboring sites will be up-steps. Therefore, for 1D arrays $\alpha = 1/2$.

Note that this argument of MW depends only on the number of up-steps, but not on their magnitude $|\Delta V|$. Thus details of the distribution of step sizes are irrelevant at $T=0$. This also holds for 2D systems, except that now the mobile charges can, to some extent, avoid up-steps. Consequently, there will be some roughness in the front of charges advancing across the array below threshold. Equation (1) still holds, with N now the distance across the gap between the electrodes. $N\alpha$ is the number of up-steps in the path across the array with the least number of up-steps ("optimal path"). The value of α in 2D will be smaller than in 1D and depend on the array topology. Unfortunately, analytical arguments that would predict α for 2D systems are not known and one has to resort to computer simulations. Specifically, for a close-packed triangular arrangement of spheres we find $\alpha = 0.226$ (see Sec. IV).

In order to model the effect of finite temperature on the global threshold for conduction, we start by considering thermal fluctuations at the local, single junction level. Let ΔE denote the change in the electrostatic potential energy of the system when a single electron moves from one site to another. If $|\Delta E| \gg k_B T$, the nonlinear, Coulomb blockage dominated current-voltage characteristic will survive: current will be suppressed below the local voltage threshold but will rise approximately linearly above it.[16] On the other hand, for $|\Delta E| \ll k_B T$, the Coulomb blockade vanishes and the junction conductance will exhibit linear, Ohmic behavior down to the lowest bias voltage.

As a first approximation, we now coarse-grain the system into two categories of tunnel junctions. Junctions between

sites with energy differences $|\Delta E| > b k_B T$ will be treated as if $T=0$, implying a fully nonlinear response and, below threshold, the absence of zero-bias conductance. Junctions between sites with energy differences $|\Delta E| < b k_B T$ will be treated as if $\Delta E = 0$ and all Coulomb blockade effects were removed, implying a linear response like Ohmic conductors. The parameter b measures the extent of thermal broadening and depends on details of the electronic level distribution. If energy levels are within $b k_B T$, then electrons from thermally excited states above the Fermi level on site i can tunnel directly into available states below the Fermi level on neighboring site j. This means that up-steps within $b k_B T$ are effectively removed.

To determine b, we consider in each nanoparticle the width of the tail of unoccupied states below and of occupied states above the Fermi level. Each tail has an approximate width of $k_B T$ so that $|\Delta E|$ is reduced by roughly $2k_B T$ and thus $b \approx 2$. To make this argument more quantitative, we consider the mean energy of states above the Fermi energy μ in particle i,

$$\langle E_{\text{high}} \rangle_i = \frac{\displaystyle\int_{\mu_i}^{\infty} E D(E) f(E) dE}{\displaystyle\int_{\mu_i}^{\infty} D(E) f(E) dE},$$

where $D(E)$ is the density of states and $f(E)$ is the Fermi-Dirac function. Evaluating the integral as a series and determining the coefficients numerically, we obtain $\langle E_{\text{high}} \rangle_i \approx \mu_i + 1.2 k_B T$. By symmetry, the mean energy of the low-energy unoccupied tail in particle j will be $\langle E_{\text{low}} \rangle_j \approx \mu_j - 1.2 k_B T$. Tunneling from the high-energy tail of particle i to the low-energy tail of particle j thus will cost a mean energy $\Delta E = (\mu_j - \mu_i) - 2.4 k_B T$. This leads to $b = 2.4$.

As temperature is raised, more and more junctions will satisfy $|\Delta E| < b k_B T$ and lose their nonlinear behavior. We define $p(T)$ as the fraction of junctions that has been effectively linearized. Since both up- and down-steps will be affected equally by thermal smearing, $p(T)$ can be found from

$$p(T) = 2 \int_0^{b k_B T} P(\Delta E) d\Delta E \tag{2}$$

if the distribution of step heights, given by the probability density $P(\Delta E)$, is known. The process of linearizing will happen randomly throughout the array until, at some temperature T^*, sufficiently many junctions have been replaced by Ohmic conductors that a continuous path involving only such conductors spans the array. At this point, the overall response will necessarily also be linear and the threshold must have reached zero: $V_t(T^*) = 0$.

An upper limit on when this point is reached can be obtained from percolation theory by considering the two classes of junctions as two types of bonds between neighboring sites. At small overall bias, we can label the nonlinear junctions as insulators and the Ohmic ones as conductors. If a (temperature-dependent) fraction $p(T)$ of all junctions in the array has been linearized, and in the absence of correla-

tions between neighboring junctions, the first continuous path of linear conductors across the array occurs, on average, at a critical fraction p_c. Here p_c is the bond percolation threshold which depends only on lattice topology and dimension (for corrections due to correlations see Sec. IV). Using Eq. (2), we thus find T^* through

$$p(T^*) = p_c. \tag{3}$$

As a consequence of these considerations, the global threshold will be a decreasing function of temperature and approach zero as $p \rightarrow p_c$. Hence, to first order,

$$V_t(T) = V_t(0)[1 - p(T)/p_c]. \tag{4}$$

In order to proceed and find the linearized fraction of junctions, $p(T)$, we need to know more about the actual distribution $P(\Delta E)$ of energy costs. It will be calculated in detail in Sec. III. However, a few important aspects are already clear from Eq. (2). In particular, since $p_c/2$ is no larger than $1/4$ for 2D lattices,[19] we have to integrate over only a small portion of $P(\Delta E)$ in order to reach a significant suppression of the threshold. If $P(\Delta E)$ does not change much over this range, we find

$$p(T) \approx 2bk_BTP(0) \tag{5}$$

and $p(T)$ is proportional to temperature. The relevant energy scale, $1/P(0)$, can be thought of as an effective charging energy, while b depends only on the shape of the internal energy distribution of the metal particle and thus is independent of topology, dimensionality and the effects of coupling.

We will see in Sec. III that this is a reasonable approximation not only for the case of zero capacitive coupling, but even more so when nearest neighbor coupling is included. Physically this is so because coupling flattens out the polarization-induced disorder in the energy landscape and small energy costs become more probable so that $P(\Delta E)$ decays slower for small ΔE. Combining Eqs. (4) and (5) we see that the normalized threshold decays linearly with temperature according to

$$\frac{V_t(T)}{V_t(0)} = 1 - 4.8k_BTP(0)/p_c, \tag{6}$$

where we have used the result $b = 2.4$ obtained earlier. In analogy with the $T=0$ result Eq. (1), the right-hand side of this equation represents $\alpha(T)/\alpha$, the temperature-dependent number of up-steps in the optimal path normalized by the number at zero temperature.

Equation (6) is a central result of this paper. It predicts a linear depression of the global threshold with temperature, with a prefactor $2bk_BP(0)/p_c$ that is universal and does not depend on the details of the threshold distribution.

III. ENERGY COST DISTRIBUTION INCLUDING NEAREST-NEIGHBOR COUPLING

To calculate $P(\Delta E)$, we start from the electrostatic energy of a system of capacitors,
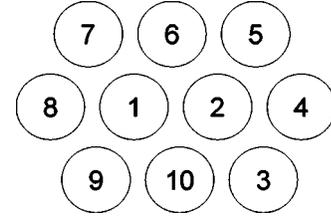

FIG. 1. Ten-sphere subsystem in a triangular lattice. The electron transfer occurs between sites 1 and 2. The other sites are the nearest neighbors.

$$E = \frac{1}{2}\sum_{i,j} (q_i + Q_i)\mathbf{C}_{ij}^{-1}(q_j + Q_j), \tag{7}$$

where the q_i are quenched, offset charges and the Q_i are mobile charges (equal to an integer multiple of $e = -1.6 \times 10^{-19}$ C or zero). The $\mathbf{C}_{ij}^{-1}$ are elements of the inverse capacitance tensor. Note that $\mathbf{C}_{11}^{-1}$, in the standard definition of the capacitance tensor, does include contributions from coupling to nearest neighbors if such coupling is present.

We define the energy difference before/after tunneling of a single electron from site 1 to site 2 as

$$\Delta E = E_{Q_1=0,Q_2=e} - E_{Q_1=e,Q_2=0}. \tag{8}$$

In the absence of any quenched charge disorder ($q_i=0$) we have $\Delta E=0$, and there is no cost associated with moving charges around inside the array. In other words, there is no Coulomb blockade of tunneling (even though $\Delta\mu_j > 0$) and the current-voltage characteristic will be linear.

Now imagine a flat, random distribution of quenched polarization charges in the range $q_i \in [-e/2, +e/2]$. As before, this range suffices because larger offsets will be compensated by mobile charges of magnitude e. In the limit of negligible capacitive coupling between sites considered for now, this leads to

$$\Delta E = e(q_1 - q_2)\mathbf{C}_{11}^{-1}.$$

To deal with nearest-neighbor capacitive coupling, we focus here on the case of a close-packed, triangular lattice simply for the sake of having a concrete picture in mind and for direct comparison with experiments. In general, any lattice type can be treated the same way and the differences affect only the quantitative results for the capacitance tensor elements.

We consider a subset of the triangular lattice consisting of 10 spheres: two central sites (1 and 2) participating in the tunneling event and their 8 surrounding neighbors as in Fig. 1. Keeping only nearest neighbor elements and taking $Q_j = 0$ for $j > 2$,

$$\Delta E = e(q_1 - q_2)(\mathbf{C}_{11}^{-1} - \mathbf{C}_{12}^{-1})$$
$$+ e\mathbf{C}_{12}^{-1}(q_3 + q_4 + q_5 - q_7 - q_8 - q_9).$$

Defining $\gamma \equiv \mathbf{C}_{12}^{-1}/\mathbf{C}_{11}^{-1}$, we write ΔE as

$$\Delta E = e^2 \mathbf{C}_{11}^{-1}\{[1-\gamma](q_1-q_2) + \gamma(q_3+q_4+q_5-q_7-q_8-q_9)\}. \tag{9}$$

The terms in parentheses, containing the q_i, are sums of 2 or 6 random variables. The maximum value for ΔE is achieved if the appropriate limiting values ($+e/2$ or $-e/2$) are inserted for the q_i. This gives

$$\Delta E_{\max} = e^2 \mathbf{C}_{11}^{-1}(1+2\gamma).$$

Without capacitive coupling to neighbors, $\Delta E_{\max}$ can be written as $\Delta E_{\max} = e^2/C_0$, where $C_0 = 4\pi\epsilon\epsilon_0 r$, is the capacitance of a single sphere of radius r embedded in a medium of dielectric constant ϵ. The key points emerging from Eqs. (8) and (9) are that the system energy cost associated with a tunnel event is not equivalent to the change in chemical potential of a single site, and that existence of a range of polarization charges q_i gives rise to a distribution of energy costs ΔE.

To calculate the full distribution $P(\Delta E)$ of energy differences, we need to first find the distributions $P_2(x)$ and $P_6(x)$ resulting from the addition of 2 or 6 random variables. In general, the probability of obtaining a value $x = x_1 + x_2 + \cdots + x_n$ from the sum (or difference) of n independent random numbers x_i can be calculated from their recursion relation:

$$P_n(x) = \int_{-\infty}^{\infty} dX' P_{n-1}(x-x') P_1(x').$$

Using Fourier transform to convert the convolution into a product, we get $P_n(\xi) = P_{n-1}(\xi) P_1(\xi)$. This leads to $P_n(\xi) = P_1^n(\xi) = [\sin(\xi/2)/(\xi/2)]^n$, or

$$P_n(x) = \frac{2}{\pi} \int_0^{\infty} \frac{\sin^n \xi}{\xi^n} \cos(2\xi x) d\xi.$$

Specifically, for $n=2$ and $n=6$ this integral can be solved analytically and gives

$$P_2(x) = (|x-1| + |x+1| - 2|x|)/2,$$

$$P_6(x) = (|x-3|^5 + |x+3|^5 - 6|x-2|^5 - 6|x+2|^5 + 15|x-1|^5 + 15|x+1|^5 - 20|x|^5)/240.$$

The probability distribution of ΔE in Eq. (9) is then given by

$$P(\Delta E) = \frac{1}{e^2 \mathbf{C}_{11}^{-1}} \int_{-\infty}^{+\infty} \frac{1}{\gamma(1-\gamma)} P_2\left(\frac{\Delta E - \Delta E'}{(1-\gamma)e^2\mathbf{C}_{11}^{-1}}\right)$$
$$\times P_6\left(\frac{\Delta E'}{\gamma e^2 \mathbf{C}_{11}^{-1}}\right) d\Delta E'. \tag{10}$$

The shape of this $P(\Delta E)$ is triangular with apex at $\Delta E=0$. Depending on γ, the shape is rounded near the top (where $\Delta E \to 0$) and curved outward near the bottom (as $\Delta E_{\max}$ is approached). The amount of rounding/curving increases with γ (Fig. 2). Specifically, for negligible coupling ($\gamma=0$), $P(\Delta E)$ becomes the distribution of differences between two random variables
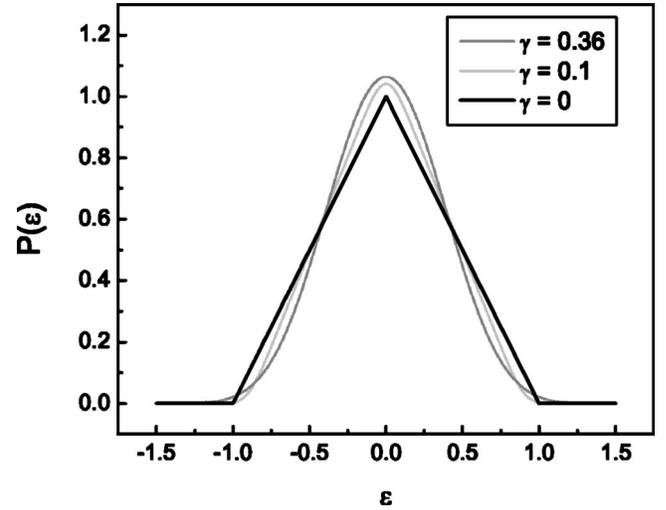

FIG. 2. Probability distribution of the energy cost of tunneling between sites 1 and 2 in Fig. 1. The distribution of $\varepsilon \equiv \Delta E/(e^2\mathbf{C}_{11}^{-1})$ is plotted where ΔE is the change in the system energy due to tunneling. $\mathbf{C}_{11}^{-1}$ is the diagonal element of the inverse capacitance matrix and $\gamma \equiv \mathbf{C}_{12}^{-1}/\mathbf{C}_{11}^{-1}$.

$$P(\Delta E) = 1/\Delta E_{\max} - |\Delta E|/(\Delta E_{\max})^2. \tag{11}$$

This is a simple triangle with $P(0)=1/\Delta E_{\max}$ and base extending from $-\Delta E_{\max}$ to $+\Delta E_{\max}$. Figure 2 shows $P(\varepsilon)$ as a function of the normalized energy cost, $\varepsilon = \Delta E/(e^2\mathbf{C}_{11}^{-1})$.

Using Eqs. (2) and (11) for $\gamma=0$, we find that the fraction of linearized junctions is

$$p(T) = \frac{2bk_B T}{\Delta E_{\max}} - \left(\frac{bk_B T}{\Delta E_{\max}}\right)^2. \tag{12}$$

For a 2D triangular lattice $p_c=0.347$ so that the temperature at which an Ohmic conducting path percolates across the lattice, defined in Eq. (3) by $p(T^*)=p_c$, is reached at $bk_B T^*/\Delta E_{\max}=0.192$. This value is small enough that, to good approximation, Eq. (5) holds and the quadratic term in Eq. (12) can be neglected for all $T<T^*$.

For finite capacitive coupling between nearest neighbors, $\gamma>0$, $P(\varepsilon)$ in Eq. (10) can be expanded around $\varepsilon=0$ to obtain

$$P(\varepsilon) = P(0) - \frac{0.55}{\gamma(1-\gamma)^3}\varepsilon^2 + O(\varepsilon^3). \tag{13}$$

The linear term disappears because the distribution has a rounded top near $\varepsilon=0$ (Fig. 2). Consequently, corrections to Eq. (5) are of order $(bk_B T^*/\Delta E_{\max})^3$ and thus smaller than in the case of zero coupling (see Sec. IV for numerical integration results for T^*). Therefore, the linear decrease of V_t with temperature in Eq. (6) holds to even better approximation. The first term, $P(0)$, in Eq. (13) can be found straightforwardly from the integral in Eq. (10) as long as γ is sufficiently small. This leads to

$$P(0) = \frac{1}{e^2 \mathbf{C}_{11}^{-1}} \left[\frac{1}{1-\gamma} - \frac{2\gamma}{(1-\gamma)^2} \int_0^\infty x P_6(x) dx \right]$$

and finally

$$P(0) \approx \frac{1}{e^2 \mathbf{C}_{11}^{-1}} \frac{1 - 1.57\gamma}{(1-\gamma)^2}. \qquad (14)$$

Note that $P(0)$ depends only on the geometry of the system and is independent of all details of the quenched charges (as long as they can be assumed uniformly random). This allows us to obtain $P(0)$ from calculations of the capacitance tensor elements $\mathbf{C}_{11}^{-1}$ and $\mathbf{C}_{12}^{-1}$. In Sec. IV we present numerical results for a range of coupling strengths and show how these tensor elements depend on the ratio of center-to-center distance, L, to particle radius, r. As particles get closer and $L/r \to 2.4$, γ reaches 0.4 and the approximation leading to Eq. (14) breaks down [see also Fig. 9(a) below]. Furthermore, for very large interparticle coupling, next-nearest-neighbor interactions will become significant and correlations between energy steps may become more important.

We can repeat the above derivation of $P(0)$ for a one-dimensional linear chain of particles. In this case, we consider 4 sites in a row with an electron moving between the two central sites. Now $P(\Delta E)$ contains the integral of a product of two P_2 functions. We find that for $\gamma < 1/3$,

$$P(0)_{1D} = \frac{1}{e^2 \mathbf{C}_{11}^{-1}} \frac{1 - 4\gamma/3}{(1-\gamma)^2}. \qquad (15)$$

One final aspect concerns how the zero-temperature threshold $V_t(0)$ in Eq. (1) is affected by capacitive coupling between neighboring particles. In MW's argument leading to Eq. (1) for the uncoupled case, the factor e/C_0 came from an increase in local potential corresponding to one full electronic charge. With capacitive coupling, the increase in local potential due to an electronic charge will be less as it effectively spreads out over the neighbors.

In order to reach the threshold for conduction, we still have to add approximately one electron to the array for each up-step in a path. To first order, the average local change in potential associated with adding an electron is $e\mathbf{C}_{11}^{-1}$, where $\mathbf{C}_{11}^{-1}$ decreases with increasing coupling. As before, α is the number of up-steps in the optimal path at $T = 0$ divided by the length of the array. The optimal path is the one with the fewest number of up-steps. Let us define V_0 as the average increase in external bias required to overcome an up-step. We then can think of the voltage threshold as a product of two quantities: the number of up-steps (αN) and the cost in bias per up-step $(V_0 \approx e\mathbf{C}_{11}^{-1})$. Modifying Eq. (1), we are led to

$$V_t(0) = \alpha N V_0 \approx \alpha N e \mathbf{C}_{11}^{-1}. \qquad (16)$$

Note, however, that this relation is only an approximation and that a full calculation is a formidable problem for $\gamma > 0$. The reason is that now local changes in potential depend strongly on the quenched charge configuration as well as on other mobile charges arriving on nearby particles. In 2D, in particular, this complex interaction poses a challenge not only for analytical calculations but also for simulations. On the other hand, 1D simulations can be carried out straightforwardly and can be used to gauge the validity of Eq. (16). This will be done in the next section.

IV. NUMERICAL CALCULATIONS AND CHECKS

In order to use Eqs. (6) and (16) we need to know certain elements of the inverse capacitance matrix as well as the value of α appropriate for a given lattice. Both of these can be obtained from numerical calculations as we detail in this section. In addition, simulations allow us to perform a number of checks of the assumptions underlying the model developed in Sec. III and they provide a direct test for the effect of correlations that were neglected in its derivation. In the following figures, we normalize capacitances by the capacitance, C_0, of an isolated sphere and energies by e^2/C_0, the maximum energy cost for tunneling between capacitively uncoupled particles.

Inverse capacitance matrix. To calculate the capacitance matrix of the 10-sphere system in Fig. 1, we used FASTCAP, a capacitance extraction program developed at MIT.[20] The program implements a preconditioned, adaptive, multipole-accelerated 3D capacitance extraction algorithm developed by Nabors *et al.*[21] Each site in the system was represented by a spherical, 1200-panel polygon. Center-to-center distances between 2.1 and 20 times the radius were examined. (For $L/r = 20$, we used a 104-panel sphere approximation so as to not run out of computer memory.) The output of the program is a 10×10 capacitance matrix $\mathbf{C}$ in units of pF for spheres of radius 1 m. We then inverted this matrix in Mathematica to find $\mathbf{C}^{-1}$. Since capacitance is directly proportional to the scale of the system, and to the dielectric constant, we can remove these dependences by scaling all capacitance elements by the self-capacitance of an isolated sphere. We will do this in all the figures to give a general result.

Figure 3 shows the effect of coupling on the 1-1 and 1-2 elements of the inverse capacitance matrix. Note that the self-capacitance $\mathbf{C}_{11}$ and thus $\mathbf{C}_{11}^{-1}$ depends on interparticle coupling because nearby spheres can polarize when a charge is added to the central sphere, decreasing the overall energy cost of the charge addition. However, as Fig. 3 shows, for values of $L/r > 3$ the change in $\mathbf{C}_{11}^{-1}$ due to nearest-neighbor coupling is small, and $\mathbf{C}_{11}^{-1}$ remains within 10% of $1/C_0$. Typical experimental values for close-packed, dodecanethiol-coated 6 nm particles give values L/r of about 2.7.[12] As Fig. 3 shows, the off-diagonal element $\mathbf{C}_{12}^{-1}$ depends less strongly on L/r than the diagonal element. Thus, the increase in γ with decreasing L/r below a value of about 3 is largely due to $\mathbf{C}_{11}^{-1}$.

We also note that the interparticle capacitance $\mathbf{C}_{12}$ depends on having extra neighbors. For example, for $L/r = 2.67$, $\mathbf{C}_{12}$ in the 10-sphere system of Fig. 1 is only 71% of the value obtained for two isolated spheres. Thus it is essential to look at the system as a whole and not to assume isolated spheres. In order to check whether or not the 10-sphere system is sufficient, we added another ring of spheres to Fig. 1, creating a 24-particle subset of the triangular array. We then calculated the full capacitance matrix for the 24-
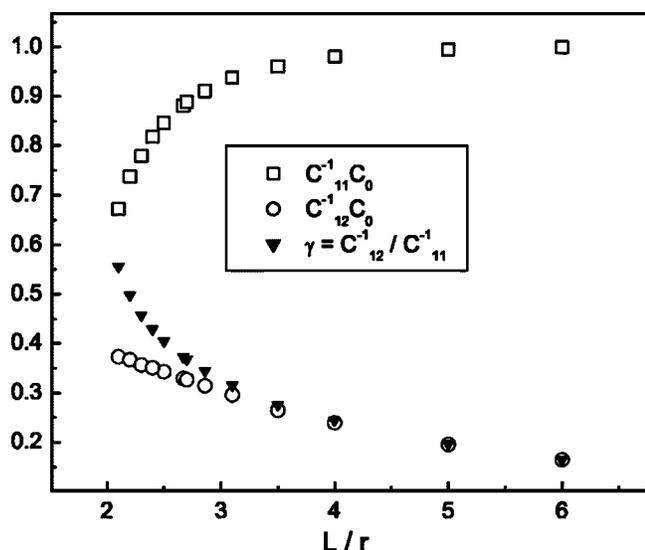
FIG. 3. Effect of coupling on the elements of the inverse capacitance matrix for a 10-particle triangular system. Coupling increases as the center-to-center spacing, L, normalized by the radius, r, decreases. As coupling increases, the inverse self-capacitance, $\mathbf{C}_{11}^{-1}$, decreases and the inverse interparticle capacitance, $\mathbf{C}_{12}^{-1}$, increases. We normalize by the self-capacitance of an isolated sphere, C_0, to assure that the values plotted are independent of r and the dielectric constant.

particle system. For $L/r=2.1$, we found that the changes in $\mathbf{C}_{11}$ and $\mathbf{C}_{12}$ are less than 1%. Consequently, we take the 10-sphere system as a sufficiently good approximation to the triangular array.

The results of the capacitance matrix calculation are in contrast to approximations[6] which estimate the effect of capacitive coupling by adding to the capacitance of an isolated single particle, C_0, the interparticle capacitance C_{12} for each neighbor. In particular, over the range $2.1<L/r<4$ the estimate $\mathbf{C}_{11}\approx C_0+6C_{12}$ for a triangular lattice gives about twice the value for $\mathbf{C}_{11}$ obtained numerically using FASTCAP.

In principle, FASTCAP will give the full capacitance matrix of the 10-particle system in Fig. 1, and thus take into account several longer range couplings. However, here we limit the discussion to nearest-neighbor coupling. First, we examine the zero-temperature limit.

Conduction threshold at $T=0$. To calculate numerically the onset of conduction at $T=0$, we follow MW's model and look for paths across the array that minimize the number of up-steps. For this, we use a variant of the well-known Dijkstra optimal path finding algorithm, the "bottleneck algorithm."[22] For each site, we define an offset charge q_i. If $q_i>q_j$, then i-to-j is considered an energy up-step in the uncoupled case. While we cannot use this method to find the full current-voltage characteristics, it provides a very fast and effective way of determining the validity of Eq. (1) and it allows us to extract the geometrical prefactor α. As defined in Sec. III, α is the number of up-steps in the optimal path at $T=0$ divided by the length of the array. Note that our definition of α differs from MW who define $\alpha=V_t(0)C_0/Ne$. The two definitions only agree in the uncoupled case.

We can also numerically obtain the charge front as it propagates across the array for voltages below threshold. To
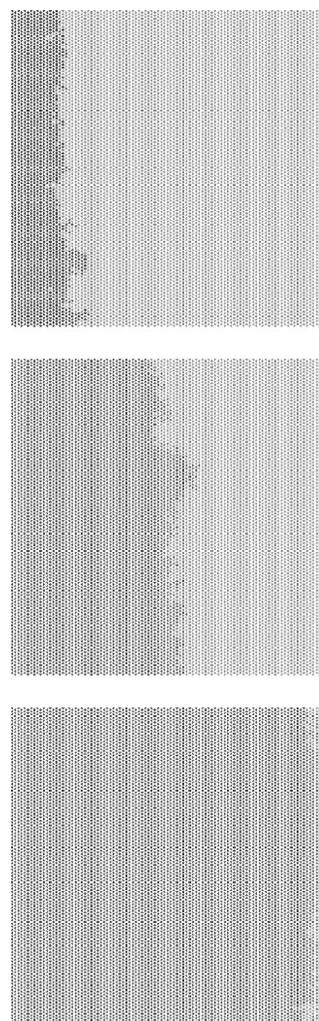

FIG. 4. Charge front in a 2D triangular lattice as a function of external bias. The mobile charges, shown in dark gray, are able to penetrate further into the array from a reservoir on the left as bias is increased from top to bottom in the 3 pictures. The simulations on a 100×100 array were carried out using the "bottleneck" algorithm from Ref. 22.

do so, we find all the sites that can be reached in less than a given number of energy up-steps. In Fig. 4 we show three snapshots from a simulation on a triangular lattice with increasing bias from left to right. The advancing charge front is seen as the right-hand edge of the dark gray region.

Let us first consider the uncoupled case. For all types of lattices investigated, we find that $V_t(0)$ increases linearly with N, as predicted by Eq. (16). For a 2D square lattice MW reported $\alpha=0.338(1)$ using Monte Carlo simulations. The bottleneck algorithm gives $\alpha=0.329(7)$ for a 160×160 square lattice (averaged over 1000 trials). For honeycomb and triangular arrays (100×100 array, 1000 trials) we find $\alpha=0.301(9)$ and $\alpha=0.226(8)$, respectively.

What is the effect of coupling on the number of up-steps in the optimal path? A "step" ΔE between two sites is not just $(q_i-q_j)/C_0$, but now takes into account all neighbors, as in Eq. (9). However, since α does not depend on the magnitude of the up-steps, we do not expect a large effect. This is
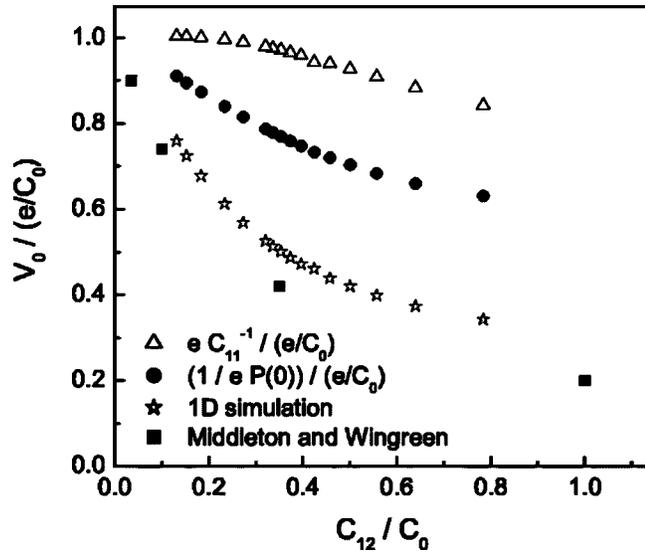
FIG. 5. Average external voltage bias per up-step, V_0, at threshold in a 1D chain of spheres as a function of interparticle coupling at $T=0$. The vertical axis is normalized by the bias per up-step in the uncoupled case, e/C_0, where C_0 is the self-capacitance of an isolated sphere. The horizontal axis is the interparticle capacitance, C_{12}, normalized by C_0. The data from our 1D simulation (open stars) are compared with simulation results from Ref. 1 (full squares) and two analytical approximations (open triangles and filled circles).

borne out by the simulations. In 1D, α is not affected by coupling even for $\mathbf{C}_{12}/\mathbf{C}_{11} \geqslant 1$. In a 2D triangular array, we find that α depends only weakly on coupling. For $L/r=2.1$, α decreases by about 10% from its uncoupled value; for $L/r \geqslant 5$, α has essentially the uncoupled value of 0.226.

In order to compare our model more directly with literature results for the global threshold in the coupled case, which are available only in 1D,[1] we simulated a 1D chain of sites. In this simulation, we only consider self-capacitance ($\mathbf{C}_{11}^{-1}$) and nearest-neighbor capacitance ($\mathbf{C}_{12}^{-1}$). An electron moves forward from site i to $i+1$ if $\Delta E_{i \to i+1} < 0$, where ΔE is calculated from Eq. (7) considering both offset charges q and integral charges Q from all previous tunneling events on all sites.

The external bias is raised in increments much smaller than $e\mathbf{C}_{11}^{-1}$ to inject electrons into the system. Electrons are allowed to propagate forward and rearrange to find the minimum energy state of the system before increasing the bias again. V_t is the external bias value for which the first electron reaches the far end of the chain. For each disorder realization in a 100-site chain, we count the number of up-steps and then raise the bias to find the threshold. As mentioned in the previous section, for finite coupling, there is no unique cost in bias per up-step, but rather a distribution. Fitting the average cost, V_0, to a quadratic function for $\gamma < 0.4$, we find

$$V_0 \frac{1}{e\mathbf{C}_{11}^{-1}} = 1 - 1.93\gamma + 1.53\gamma^2 + O(\gamma^3). \qquad (17)$$

Results from this simulation are shown in Fig. 5, where we plot the average cost per up-step, V_0, normalized to the

uncoupled value, as a function of $\mathbf{C}_{12}/C_0$ in a 1D chain. This is compared to the approximations $V_0 \approx e\mathbf{C}_{11}^{-1}$ from Eq. (16) and $V_0 \approx 1/eP(0)$ using the 1D result, Eq. (15) for $P(0)$. Also shown are four data points from MW's Fig. 1, based on a full simulation of the current-voltage characteristics of a chain. (Note that MW use a different normalization in their Fig. 1, i.e., they plot $V_t C_0/eN$, and extend the simulations to larger coupling strengths.)

Conduction threshold for $T>0$. As a next step, we add temperature to the simulations. In the 2D algorithm that finds the optimal path across the array we have direct access to all bonds, and thus energy costs, ΔE, for moving an electron between any pair of neighboring sites. This allows us to test the validity of the linear decrease of the threshold with increasing temperature predicted by Eq. (6). As temperature increases, steps with magnitudes smaller than a threshold energy, $\Delta E_{\text{th}} = bk_B T$ are thermally erased. In the path-finding algorithm, we count all steps less than ΔE_{th} as "down-steps," that is, they do not cost any energy. We then traverse the energy landscape to find the least-cost path as before. Figure 6 shows three snapshots from the simulation. The threshold ΔE_{th}, and thus temperature, is increased from left to right. In dark gray we show all sites reachable without cost from the left edge.

In Fig. 7 we plot $\alpha(T)$ as a function of the effective temperature, ΔE_{th}, for various degrees of coupling. In all cases, we find that the number of up-steps in the optimal path decreases with increasing threshold energy approximately linearly. [The deviations from a strictly linear decrease, close to $\alpha(T)=0$, come from a finite size effect: the simulated arrays contained 100×100 sites, so around $\alpha(T)=0.01$, the average number of up-steps reaches 1, below which the average is fractional and thus no longer a physical measure.] We also see that for a given "temperature" the threshold decreases with increasing coupling. Furthermore, the temperature T^* at which $\alpha(T)=0$ decreases with increasing coupling [see also Fig. 9(b)]. In accordance with the results in Fig. 3, these trends are most pronounced for small L/r and saturate near the uncoupled behavior for $L/r > 5$.

Percolation and correlations. In the analytic calculation of T^* in Sec. II, we found the fraction of linearized bonds, $p(T)$, through Eq. (2) and defined T^* as $p(T^*)=p_c$, where p_c is the bond percolation threshold in the lattice under consideration. This procedure relies on two assumptions that we now test.

First, the basic idea of our tunneling model is that none of the down-steps cost energy. Implicit in Eq. (2) is a somewhat more restrictive criterion, namely $|\Delta E| < bk_B T$, requiring that the path be along only those bonds (corresponding to either up- or down-steps) that had been linearized by thermal fluctuations. There may be energetically much more optimal, but more asymmetric, paths that take advantage of those larger-energy down-steps that have not yet been linearized. In this situation, we are starting with a lattice with all down-steps in place and ask when the system-spanning path forms in the process of adding up-steps of increasing size.

Second, setting $p(T^*)=p_c$ and using literature values for p_c assumes that the usual rules for bond percolation apply and, in particular, all bonds are placed completely randomly.

FIG. 6. Effect of temperature on an 2D triangular array with quenched charge disorder. As temperature is increased from top to bottom in the 3 pictures, mobile charges (in dark gray) can penetrate deeper into the array without energetic cost. When a percolating dark gray path spans the array from left to right, the global threshold bias for conduction reaches zero. The simulations on a 100×100 triangular array were carried out using the "bottleneck" algorithm from Ref. 22.

However, while the site energies are from a flat distribution, the energy differences between sites are correlated. For example, in the triangular lattice in Fig. 1, the energy differences between sites 1 and 2 and between sites 2 and 6 completely specify ΔE between sites 1 and 6. Therefore, p_c may not necessarily provide an accurate value for the threshold. Finally, even in the absence of correlations, the finite size of arrays corresponding to experimental situations (with N no more than a few 100) may lead to a small correction to p_c as listed for infinite lattices.

We investigated these questions for a variety of lattice types by calculating numerically the threshold p_a, defined as the average fraction of bonds required for percolation under the *asymmetric* condition $\Delta E < bk_B T^*$, and the threshold p_s, defined as the average fraction of bonds required for percolation under the *symmetric* condition $|\Delta E| < bk_B T^*$. Both are listed in Table I, together with p_c as obtained from the same
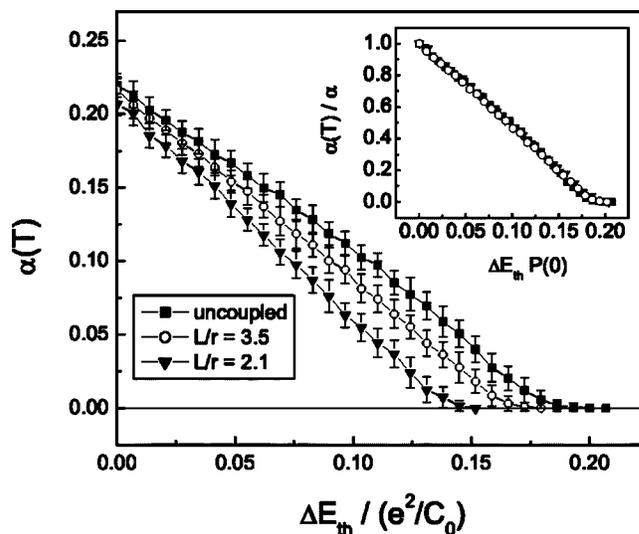

FIG. 7. Decrease of the number of energy up-steps in the optimal path with temperature. $\alpha(T)$ is defined as the temperature-dependent number of up-steps in the least cost path across the array divided by the array length. The effect of thermal fluctuations is introduced by counting up-steps only if they exceeded a cutoff energy $\Delta E_{th} = bk_B T$. Data are shown from simulations on a 2D triangular lattice containing 100×100 spherical particles for three different coupling strengths, parametrized by the ratio of center-to-center distance, L, to sphere radius, r. The inset shows the collapse of the curves upon normalization by $\alpha \equiv \alpha(T=0)$, and by $1/P(0)$, the relevant energy scale for temperature dependence.

lattice but with randomly assigned bond energies rather than random site energies. z is the coordination number, the number of nearest neighbors of each site. The lattice with $z=2$ consists of 200 parallel 1D wires.

In Fig. 8, a comparison between p_s and p_c gives a sense of the relevance of correlations which increase p_s roughly lin-

TABLE I. Percolation coefficients for different coordination numbers z, calculated for 200×200 arrays and averaged over 200 trials. p_s is the average fraction of bonds that need to be linearized in the whole array such that the first system-spanning path appears containing only linearized bonds (both up- and down-steps). p_a is the average fraction of bonds linearized in the array for the first system-spanning path containing nonlinearized down-steps as long as all up-steps are linearized. p_s and p_a are for systems with random site energies. p_c is the bond percolation fraction for the uncorrelated bond percolation. The theoretical values $p_{c,th}$ are taken from Ref. 19 and presented for comparison to indicate the extent of finite-size effects.

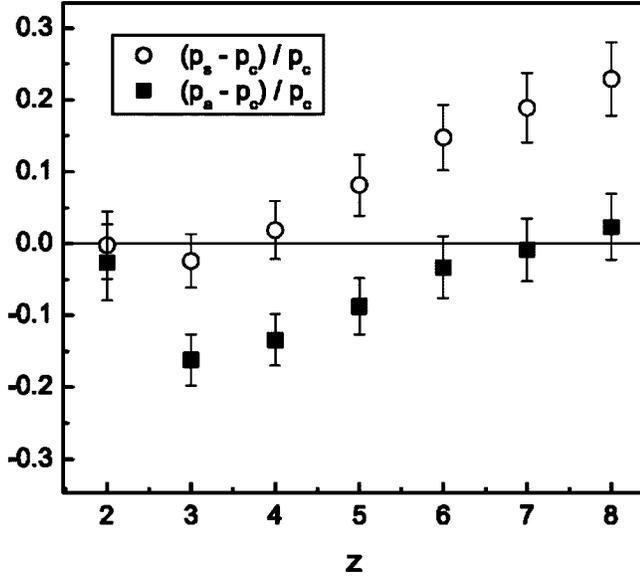| z	$p_{c,th}$	p_c	p_s	p_a
2	1	0.970(7)	0.968(39)	0.945(45)
3	0.653	0.643(9)	0.627(15)	0.539(15)
4	0.5	0.500(8)	0.509(12)	0.433(11)
5		0.420(6)	0.455(10)	0.384(10)
6	0.347	0.346(6)	0.397(8)	0.335(9)
7		0.292(6)	0.348(8)	0.289(7)
8		0.250(5)	0.307(7)	0.255(7)

FIG. 8. Comparison of symmetric and asymmetric percolation conditions for various 2D arrays with coordination numbers, z. p_s, p_a, and p_c are defined in Table I. All simulation data are for arrays of size 200×200 and averaged over 200 disorder realizations.
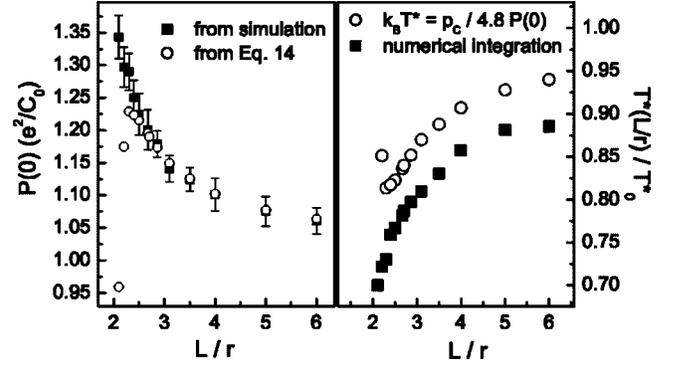

FIG. 9. Effect of capacitive coupling on the energy scales associated with the temperature dependence of the global threshold for conduction. L is the center-to-center distance between neighboring spherical particles and r is their radius. (a) Changes in the peak of the energy-cost distribution, $P(0)$, as a function of coupling. $1/P(0)$ plays the role of an effective charging energy; in this plot it has been normalized by the maximum energy cost in the uncoupled case, e^2/C_0. Results from Monte Carlo data (full squares) and from the approximation given by Eq. (14) (open circles) are shown. (b) Changes in T^*, the temperature at which the voltage threshold of the array becomes zero, for a triangular lattice (percolation threshold, $p_c=0.347$). T^* has been normalized by T_0^*, the value in the uncoupled case. Closed square symbols are data from numerical integration of the energy cost distribution, $P(\Delta E)$, as obtained by Monte Carlo simulation; open circles show the approximation given by Eq. (5).

early with increasing z (ignoring the case of $z=2$). At the same time, antisymmetric paths involving large down-steps give a threshold fraction, p_a, that is systematically lower than p_s by about 15%. Intriguingly, and quite unexpectedly, for lattices with $z=6$ to $z=8$ the contributions from correlations and asymmetry appear to cancel each other to a large extent so that p_c provides an excellent estimate of the "true" value, p_a. Thus, using p_c in Eq. (3) to estimate T^* should give very reasonable estimates for experiments on self-assembled nanoparticle layers. The small difference between the theoretical p_c and the value from the simulation shows the insignificance of finite size effects for 200×200 arrays.

Distribution of energy costs. The last approximation in the model we wish to test is the replacement of the integral in Eq. (2) with $p_c=4.8k_BT^*P(0)$. To find the full distribution of energy costs for the nearest-neighbor-coupled 10-sphere system shown in Fig. 1, we used a Monte Carlo routine. Offset charges from a uniform random distribution $[-e/2,+e/2]$ were assigned to each of the 10 sites. Using the capacitance matrix as calculated from FASTCAP, the energy cost ΔE associated with tunneling from site 1 to site 2 was found from Eq. (9) for each disorder realization. $P(\Delta E)$ was then obtained from sampling ΔE for 10^6 offset charge realizations for each value of L/r.

Figure 9(a) shows the normalized peak probability density $P(0)e^2/C_0$ as a function of L/r. $P(0)e^2/C_0$ only depends on L/r since both C_0 and $1/P(0)$ are proportional to r and ϵ. We compare the simulation value with the approximation in Eq. (14). Knowing the full distribution from Monte Carlo simulations allows us to find, without approximations, the critical temperature T^*, where the voltage threshold goes to zero. According to Eqs. (2) and (3) this is done by integrating $P(\Delta E)$ out to the point where the area under the graph corresponds to p_c. In Fig. 9(b), we compare the results of nu-

merical integration with the analytical approximation $T^* = p_c/[2bk_BP(0)]$ [Eq. (5)] with $P(0)$ from Eq. (14) for a 2D triangular lattice.

V. CURRENT-VOLTAGE CHARACTERISTICS ABOVE T^*

Next, we investigate the behavior for temperatures $T \simeq T^*$ and above. Within our model, T^* is defined as the temperature at which there are just enough local junctions linearized to span the array at zero bias and remove the global threshold. In other words, with increasing temperature the nonlinear current-voltage (I-V) characteristics, described by the powerlaw $I\sim[V-V_t(T)]^\zeta$, have been linearly shifted to the left until, at T^*, they first reach the origin with finite slope. This gives rise to a finite zero-bias conductance, $g_0 \equiv dI/dV|_{V=0}$.

For $T>T^*$, additional linearized junctions provide parallel paths across the array and the zero-bias conductance increases. For any given temperature, however, an increase in bias will eventually provide sufficiently high local voltage drops to involve portions of the array with junctions not yet linearized by thermal fluctuations. Thus, at sufficiently high bias, the I-V characteristics will change back from Ohmic to the original nonlinear powerlaw behavior with temperature-independent exponent ζ.

These considerations correspond to a picture in which the nonlinear I-V curve of a 2D array emerges from summing the contributions from all paths carrying current at a given bias voltage (this is the essence of the scaling derived by MW). As the bias is increased above $V_t(T)$, more and more paths
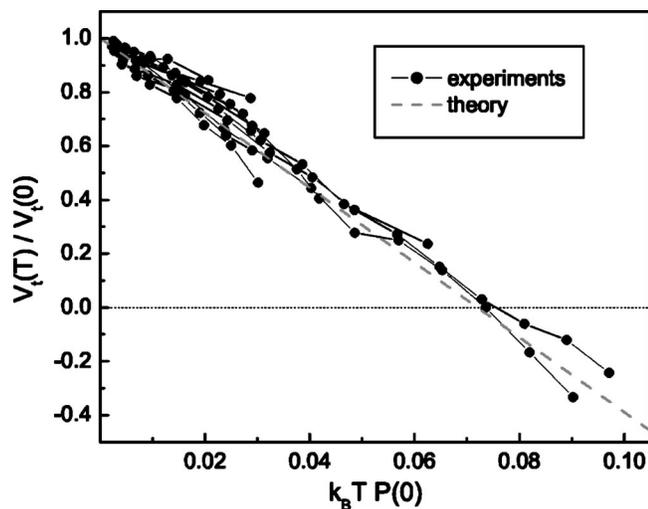
FIG. 10. Decrease of the normalized voltage threshold as a function of effective temperature variable $k_B T P(0)$ for 6 nm diameter, close-packed gold nanoparticle monolayers. (Reproduced from Ref. 12 with permission.)

will open up as their up-steps are overcome. Above T^*, when the global threshold disappears along the optimal path, there still are many other paths that have finite thresholds and are accessible at higher bias. These thresholds will keep decreasing linearly with temperature as more and more steps are linearized by thermal fluctuations. As a consequence, the high-current, powerlaw portion of the I-V curves will shift to lower and lower bias voltages.

We therefore expect the I-V curves to collapse, by a simple horizontal shift, onto a master curve not only for $T < T^*$, but, at least with their high-bias portion, also for $T > T^*$. In the latter regime a true threshold for global conduction obviously no longer exists and $V_t(T)$, as obtained from the shift required for a high-bias I-V collapse onto a common power law, should be thought of as an *effective* threshold value. This effective $V_t(T)$ will be negative for $T > T^*$.

These predictions are borne out by experiments. As first observed by Ancona *et al.*[5] and also seen in Fig. 10, the linear decrease of V_t with T continues past T^* and into a regime of negative effective threshold values. (Our simulation results in Fig. 7 are not based on calculating full I-V curves. Since our method finds the first system-spanning path, it is no longer applicable above T^* where such paths exist already at zero applied bias.)

We note that our model provides a natural explanation for this smooth crossover from positive to negative $V_t(T)$ which does not invoke additional mechanisms. In particular, it does not bring into play activation over the tunnel barriers for $T > T^*$, as proposed by Ancona *et al.*[5] Because such barriers are set by the properties of the alkanethiol ligands separating adjacent nanoparticles, we expect barrier heights in excess of several eV, corresponding to the first available electronic states in the ligands. This is significantly higher than either $k_B T$ or the voltage drop per up-step, making hopping over the barrier highly unlikely.

How does g_0 depend on temperature? To address this point, we revisit a simplifying approximation made in the

model, namely the coarse-graining in which nonlinearized junctions were assumed to be unaffected by thermal fluctuations and to exhibit zero conductance below threshold. In principle, of course, finite T will always induce some zero-bias conductance. For a single junction this zero-bias conductance exhibits activated behavior, i.e., is proportional to $\exp(-U/k_B T)$, where the activation energy, $U = \Delta E$, is the energy cost required to move a charge across the junction.[16]

Sufficiently far below T^*, there always will be several junctions along the optimal path with $\Delta E \gg k_B T$. Consequently, the overall zero-bias conductance will be exponentially suppressed to a level where g_0 is well approximated by the coarse-graining approximation.

Once T^* is approached, linearized junctions for the first time form a system-spanning path. g_0 will be dominated by the relatively few bottleneck junctions with the largest activation energy in the path, $\Delta E \sim k_B T^*$. The majority of paths around the bottlenecks would involve junctions with much larger ΔE which therefore could shunt the bottlenecks only insignificantly.[23,24]

Therefore, near T^* the overall, zero-bias array conductance, g_0, will display activated behavior similar to a single junction with $U = b k_B T^* = p_c / [2P(0)]$. As before, the key point here is that the activation energy is not simply the charging energy of an isolated grain, but is connected to the optimal path across an energy landscape established by the quenched charge disorder. For 2D triangular arrays $p_c/2 \sim 0.17$ so that U is approximately $1/5$ of the effective charging energy $1/P(0)$.

Above T^*, additional paths in which all up-steps have been thermally erased will span the array. These parallel paths will contribute to g_0 and modify the behavior. Taking the number density, $D(T)$, of such paths to be proportional to the percolation conductivity of the linearized subset of junctions above p_c, we have $D(T) \sim (p(T) - p_c)^t$, where $p(T)$ is given by Eq. (2) and $t \approx 1.3$ in 2D.[19] The overall zero-bias conductance at temperature T then follows from integration of $D(T')g_0(T')$ between T^* and T. This will give a powerlaw correction to the simple activated behavior, but we expect the optimal path established at T^* to continue to dominate since its bottlenecks have the lowest activation energy of the set.

The experimental data in Ref. 12 for the zero-bias conductance in 2D arrays above T^* is compatible with simple activated behavior, with values for U that are within a factor two of $p_c / [2P(0)]$. However, since T^* can reach 100 K or more in these arrays, the remaining interval up to room temperature simply is not large enough to provide a stringent test of the model predictions. The simple activated form for g_0 was also observed by Black *et al.* in arrays of Co nanoparticles.[6]

VI. DISCUSSION

The model described in the preceding sections provides a physical picture for the role of thermal fluctuations as they affect the nonlinear transport properties in systems with random local thresholds for conduction. One key aspect is that such systems cannot be described by associating a single, fixed energy cost with charge motion from site to site. In-

stead, it is important to consider the fact that energy costs depend on both the Fermi levels of the particles involved in the tunneling process, and on the surrounding charge environment. This is the essence of Eq. (8), which gives the change in electrostatic energy of the system as a whole, and, in the nearest neighbor approximation considered here, leads to the probability density of energy costs shown in Fig. 2.

In particular, the energetics of the system are not determined simply by the change in the Fermi level (by some fixed single electron "charging energy") of the nanoparticle tunneled into. Energy costs derive from differences in the total system energy before and after a tunneling event and thus involve at a minimum two particles or, with capacitive nearest neighbor coupling, ten particles in a 2D triangular lattice (Fig. 1) or four particles along a 1D line. In the absence of quenched charge disorder, these energy costs vanish and mobile charges can move freely inside the array (the only costs are incurred when charges enter the edges of the array from one of the electrodes). Therefore, the scaling of the global threshold with system size N in Eq. (1) (the original MW result) or its modification for finite coupling strength, Eq. (16), are a direct consequence of quenched charge disorder.

However, as far as the global threshold is concerned, the detailed shape of the full energy cost distribution turns out to be not critical. Rather, as we showed by mapping the system onto an equivalent percolation problem, the behavior is dominated by the lowest-cost percentiles (up to $p_c/2$). To very good approximation, this is captured by the zero-cost, peak value of the probability density, $P(0)$ [Eqs. (14) and (15), for 2D and 1D systems, respectively]. Increased capacitive coupling is found to have two effects: it flattens the energy landscape, thereby narrowing the width of the energy cost distribution and increasing the value of $P(0)$, and it rounds off the peak of the distribution, making $P(0)$ an even better approximation of the relevant portion of $P(\Delta E)$.

There are several predictions that emerge from the analytic model.

First, the model predicts a linear decrease of the overall, global threshold with temperature [Eq. (6)]. This decrease is directly proportional to $k_B T P(0)$, the strength of thermal fluctuations measured relative to the effective charging energy $1/P(0)$. What is particularly appealing about this result is that all details about capacitive coupling and particle geometry enter through $P(0)$, while the numerical prefactor, $4.8/p_c$, captures the underlying network topology and dimension through the percolation threshold, p_c. Therefore, data from systems with similar structure but different particle sizes, spacings, or dielectric constants should collapse onto a "universal" curve when plotted as $V_t(T)/V_t(0)$ versus $k_B T P(0)$.

Second, for sufficiently broad distributions of quenched charge disorder we expect that thermal fluctuations do not alter the basic character and roughness of the energy landscape. Thus we expect MW's zero-temperature powerlaw scaling of the nonlinear current-voltage (I-V) characteristics, $I \sim [V - V_t(0)]^\zeta$, to survive at finite T with fixed exponent ζ, but with $V_t(0)$ replaced by $V_t(T)$. In other words, the shape of the I-V characteristics remains unaffected by temperature

while they are shifted linearly towards smaller threshold values.

Third, the threshold is expected to vanish and the nonlinear, Coulomb-Blockade-type current voltage characteristics are expected to change to linear, Ohmic behavior near zero bias once the temperature exceeds $T^* = p_c/[4.8 k_B P(0)]$ [Eqs. (3) and (5)].

Fourth, also for finite capacitive coupling, the zero-temperature global threshold value, $V_t(0)$, can be written as a product of two quantities: the average number of up-steps encountered along the optimal path across the array, αN, which depends mainly on array geometry, and the average applied voltage per up-step, V_0, at threshold. We argued that, at least to first order, capacitive coupling can be taken into account by $V_0 \approx e \mathbf{C}_{11}^{-1}$ [Eq. (16)] instead of e/C_0 for the uncoupled case [Eq. (1)].

The robustness of the linear decrease of the global threshold for conduction with temperature is underscored by recent simulations of the full current-voltage characteristics for mobile charges hopping between traps in a 2D lattice.[15] The charges interact via a long-range Coulomb term and the trap depth at each site is chosen from a Gaussian distribution. In this work Reichhardt and Olson Reichhardt not only find behavior qualitatively similar to our model, but also track as a function of temperature the charge flow patterns beyond threshold. Their results support a basic, underlying tenet of our approach, namely that small thermal fluctuations simply shift $V_t(T)$ to smaller values while preserving the roughness of the energy landscape and thus the shape of the current-voltage characteristics.

Conversely, such linear shift might be taken as an indicator of a sufficiently wide distribution of trapping depths or local threshold values: simulations by Rendell *et al.* of small 2D tunnel junction networks using the full, temperature-dependent "orthodox" Coulomb blockade model show this shape-preserving shift emerging once quenched charge disorder is introduced.[9]

The fact that $P(0)e^2/C_0$, through $\mathbf{C}_{11}^{-1}$ and $\mathbf{C}_{12}^{-1}$, depends only on L/r makes comparison with experiments straightforward as long as the array geometry is known. In particular, if L and r can be determined from transmission electron micrographs, Fig. 9 together with $C_0 = 4\pi\epsilon\epsilon_0 r$ give direct access to $P(0)$ for triangular arrays, and thus make it possible to plot the normalized threshold, $V_t(T)/V_t(0)$ as a function of scaled temperature, $k_B T P(0)$. Figure 10 shows such plot for temperature-dependent threshold data obtained from self-assembled, close-packed gold nanocrystal monolayers covering a range of array lengths ($27 < N < 170$) and effective charging energies $96 \text{ meV} < 1/P(0) < 302 \text{ meV}$.[12] The threshold values were obtained from linear shifts of the full I-V curves onto a single powerlaw mastercurve for each sample (with temperature-independent exponent $\zeta = 2.25 \pm 0.1$).

All of these data are seen to cluster around the linear decay with slope $-4.8/p_c = -13.8$ and x intercept $k_B T^* P(0) = p_c/4.8 = 0.07$ predicted by the model. Note that this data collapse contains no free parameters once $V_t(T)$ has been measured [over a wide enough range to extrapolate reliably to $V_t(0)$] and $P(0)$ been obtained from the array geometry. If

direct access to L and r is not possible, but N can be estimated from the electrode spacing, $P(0)$ can be estimated using Eq. (16) together with the appropriate value for α listed in Sec. IV.

The linear suppression of $V_t(T)$ with temperature was also observed by Ancona *et al.*[5] in experiments on 2D arrays of gold nanoparticles, and by Bezryadin, Westervelt, and Tinkham[14] in studies of 1D carbon nanoparticle chains. While micrographs allowing for a determination of L and r were not available from either experiment, Bezryadin *et al.* found that the voltage threshold decreased as $V_t(T) \approx V_t(0) - N k_B T / e$. The authors also give the radius of the carbon particles as well as N and $V_t(0)$. From this information we estimate a cost per up-step of about $0.2 e / C_0$. From Fig. 5 and capacitance calculations of a 4-particle 1D chain, we find $P(0) = 1.66(C_0/e^2)$. With $p_c = 1$ for a 1D chain our model gives $V_t(T) = V_t(0) - 4.8 V_t(0) P(0) k_B T$ from Eq. (6). The second term can be written as $-4.8[0.5N(0.2e/C_0)] \times (1.66C_0/e^2)k_B T$, where the term in square brackets is $V_t(0)$ and $\alpha_{1D} = 0.5$.[1] Using the experimental parameters given by Bezryadin *et al.*, our theory predicts $V_t(T) = V_t(0) - 0.8 N k_B T / e$, which is close to the experimental temperature dependence.

VII. CONCLUSIONS

Our model describes the effect of temperature on the global threshold for conduction through arrays with distributed local thresholds due to quenched charge disorder. It resolves two long-standing issues, namely how to extend the original,

$T=0$ scaling approach by MW to $T>0$ and how to include capacitive coupling between nearest neighbors.

One key finding is a robust, linear decrease of the global threshold with temperature, in excellent agreement with recent experiments on close-packed nanocrystal arrays. This explains the experimental finding that powerlaw *I-V* characteristics resulting from Coulomb blockade effects keep their nonlinear shape to remarkably high temperatures while simply being parallel-shifted as T is increased. The model further predicts the existence of a crossover temperature T^*, above which the low-voltage portion of the *I-V* characteristics changes and acquires a significant zero-bias conductance that exhibits simple activated behavior.

A second key finding is the identification of $1/P(0)$ as the relevant, effective charging energy, extending earlier results that did not treat capacitive coupling. Our approach explicitly takes into account the fact that quenched charge disorder leads to a distribution of energy costs for tunneling, even for otherwise perfect lattices of identical junctions. Finally, we present numerical calculations that allow one to extract the relevant capacitance matrix elements as well as $P(0)$ from knowledge of interparticle spacing and particle diameter.

[1] A. A. Middleton and N. S. Wingreen, Phys. Rev. Lett. **71**, 3198 (1993).

[2] A. J. Rimberg, T. R. Ho, and J. Clarke, Phys. Rev. Lett. **74**, 4714 (1995).

[3] C. Kurdak, A. J. Rimberg, T. R. Ho, and J. Clarke, Phys. Rev. B **57**, R6842 (1998).

[4] M. N. Wybourne, L. Clarke, M. Yan, S. X. Cai, L. O. Brown, J. Hutchison, and J. F. W. Keana, Jpn. J. Appl. Phys., Part 1 **36**, 7796 (1997).

[5] M. G. Ancona, W. Kruppa, R. W. Rendell, A. W. Snow, D. Park, and J. B. Boos, Phys. Rev. B **64**, 033408 (2001).

[6] C. T. Black, C. B. Murray, R. L. Sandstrom, and S. Shouheng, Science **290**, 1131 (2000).

[7] R. Parthasarathy, X.-M. Lin, and H. M. Jaeger, Phys. Rev. Lett. **87**, 186807 (2001).

[8] C. Reichhardt and C. J. Olson Reichhardt, Phys. Rev. Lett. **90**, 046802 (2003).

[9] R. W. Rendell, M. G. Ancona, W. Kruppa, E. E. Foos, A. W. Snow, D. Park, and J. B. Boos, IEEE Trans. Nanotechnol. **2**, 75 (2003).

[10] K. C. Beverly, J. F. Sampaio, and J. R. Heath, J. Phys. Chem. B **106**, 2131 (2002).

[11] J. F. Sampaio, K. C. Beverly, and J. R. Heath, J. Phys. Chem. B **105**, 8787 (2001).

[12] R. Parthasarathy, X.-M. Lin, K. Elteto, T. F. Rosenbaum, and H. M. Jaeger, Phys. Rev. Lett. **92**, 076801 (2004).

[13] A. S. Cordan, Y. Leroy, A. Goltzene, A. Pepin, C. Vieu, M. Mejias, and H. Launios, J. Appl. Phys. **87**, 345 (2000).

[14] A. Bezryadin, R. M. Westervelt, and M. Tinkham, Appl. Phys. Lett. **74**, 2699 (1999).

[15] C. Reichhardt and C. J. Olson Reichhardt, Phys. Rev. B **68**, 165305 (2003).

[16] K. K. Likharev, Proc. IEEE **87**, 606 (1999).

[17] Y. Joseph *et al.*, J. Phys. Chem. B **107**, 7406 (2003).

[18] W. Wang, T. Lee, and M. A. Reed, Phys. Rev. B **68**, 035416 (2003).

[19] B. I. Shklovskii and A. L. Efros, *Electronic Properties of Doped Semiconductors* (Springer-Verlag, New York, 1984).

[20] FASTCAP capacitance extraction program. MIT Research Laboratory of Electronics. The program can be downloaded free of charge from the developers at: http://www.rle.mit.edu/cpg/research_codes.htm.

[21] K. Nabors, S. Kim, and J. White, IEEE Trans. Microwave Theory Tech. **40**, 1496 (1992).

[22] T. H. Cormen, C. E. Leiserson, R. L. Rivest, and C. Stein, *Introduction to Algorithms*, 2nd ed. (MIT Press, Cambridge, MA, 2001).

[23] D. Berman, B. G. Orr, H. M. Jaeger, and A. M. Goldman, Phys. Rev. B **33**, 4301 (1986).

[24] A. Priolo, H. M. Jaeger, A. J. Dammers, and S. Radelaar, Phys. Rev. B **46**, 14 889 (1992).